Electronic Supplementary Information (ESI)

Synergistic Solar-Powered Water-Electricity Generation via Rational Integration of Semitransparent Photovoltaics and Interfacial Steam Generators

Qing Ji,[a] Na Li,[a] Shuxue Wang,[a] Shuai Li,[a] Fangbin Li,[a] Liangmin Yu,[b,c] Petri Murto*[,d] & Xiaofeng Xu*[,a]

[a] College of Materials Science and Engineering, Ocean University of China, Qingdao 266100, China.

[b] Key Laboratory of Marine Chemistry Theory and Technology, Ministry of Education, Ocean University of China, Qingdao 266100, China.

[c] Open Studio for Marine Corrosion and Protection, Pilot National Laboratory for Marine Science and Technology, Qingdao 266237, China.

[d] Department of Chemistry, University of Cambridge, Cambridge, CB2 1EW, United Kingdom.

* Corresponding authors: X. Xu, email: xuxiaofeng@ouc.edu.cn

P. Murto, email: pm707@cam.ac.uk

Table of Contents

1. Materials

The donor poly[(2,6-(4,8-bis(5-(2-ethylhexyl-3-fluoro) thiophen-2-yl)-benzo[1,2-b:4,5-b′] dithiophene))-alt-(5,5-(1′,3′-di-2-thienyl-5′,7′-bis(2-ethylhexyl) benzo [1′,2′-c:4′,5′-c′] dithiophene-4,8-dione)] (PM6) was prepared according to the previous literature.[1,2] The small-molecule acceptor Y6 was purchased from Solarmer Energy, Inc., China. Ferric chloride hexahydrate ($FeCl_3 \cdot 6H_2O$) was purchased from Shanghai Macklin Biochemical Co., Ltd, China. Pyrrole was purchased from Mreda Technology, Inc., China.

2. Material characterization

Density and porosity were measured by using a high-precision density meter (AU-120PF, Quarrz). Morphologies and elemental mapping were characterized by a scanning electron microscope (VEGA3, TESCAN) in combination with an energy dispersive X-ray spectrometry. 3D optical microscope images were characterized via a 3D laser scanning confocal microscope (VK-X260K, Keyence). X-ray photoelectron spectroscopy (XPS) spectra were measured with a XPS spectrometer (Thermo Kalpha). Surface wettability was evaluated by an optical contact angle meter (CA, JC2000DM, POWEREACH) combined with a camera. Absorption spectra were measured with a UV−Vis−NIR absorption spectrometer (SHIMADZU UV2600). Tensile stress−strain curve was measured using a mechanical testing system equipped with a digital force gauge (M5-100, MARK-10) and a force test stand (ESM303, MARK-10). Bacteriostatic tests were measured by using a CytoFLEX flow cytometer (A00-1-1102).

3. Fabrication of P-NC films

Cellulosic nonwoven fabrics were rinsed with acetone and deionized water, and air-dried for 24 h. After that, the nonwoven fabrics were immersed into a $FeCl_3 \cdot 6H_2O$ solution (1 mol/L) for 1 h, and then immersed into a pyrrole solution (0.2 mol/L) and vibrated via a benchtop orbital shaker for 12 h. Finally, polypyrrole (PPy)-modified nonwoven fabrics (P-NC) were obtained and washed with deionized water to remove all reagent and catalyst.

4. Water diffusion characterization

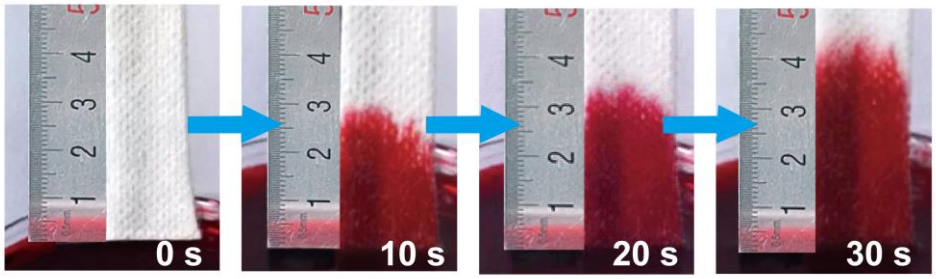

Figure S1. Water diffusion characterization of cellulosic nonwoven fabrics (or named NC film).

5. Fourier transform infrared (FTIR) characterization

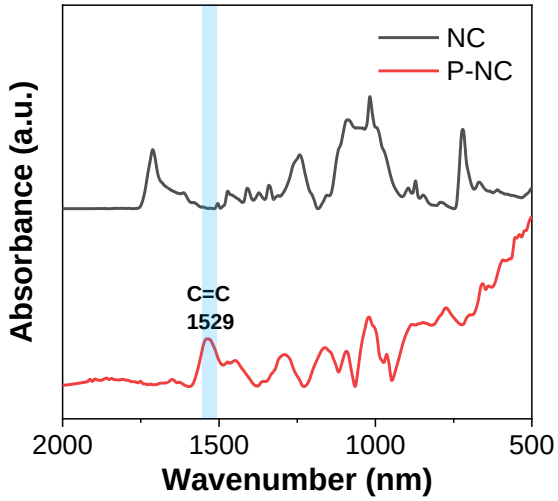

Figure S2. FTIR spectra of NC and P-NC films.

The peak at 1529 cm^{-1} corresponds to the C=C stretching of pyrrole rings, which is absent in the neat NC film.[3]

6. Thermogravimetric analysis (TGA)

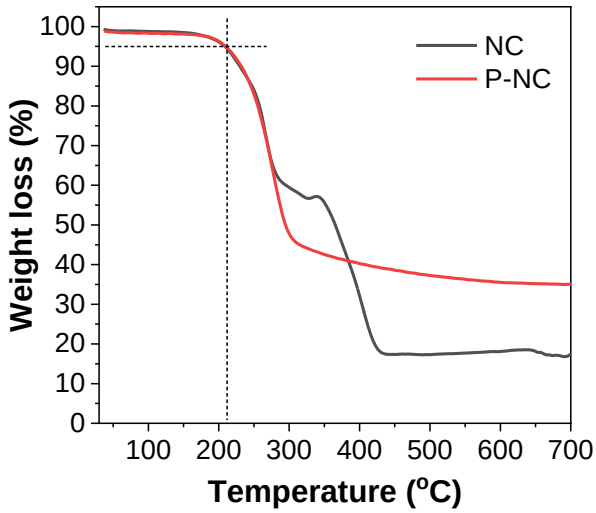

Figure S3. TGA traces of NC and P-NC films (the dotted line illustrates the temperature at 5% weight loss).

7. Durability tests of P-NC films

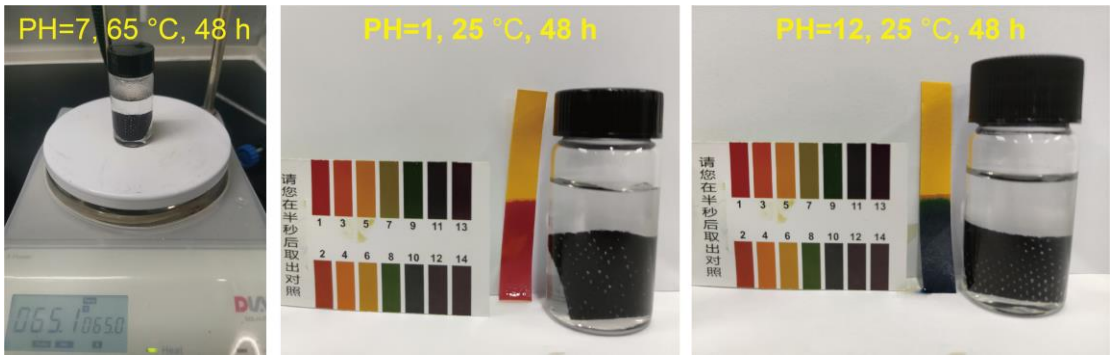

Figure S4. Digital photographs of P-NC films after soaking in hot, acidic and alkaline water.

8. Scanning electron microscope (SEM) characterization

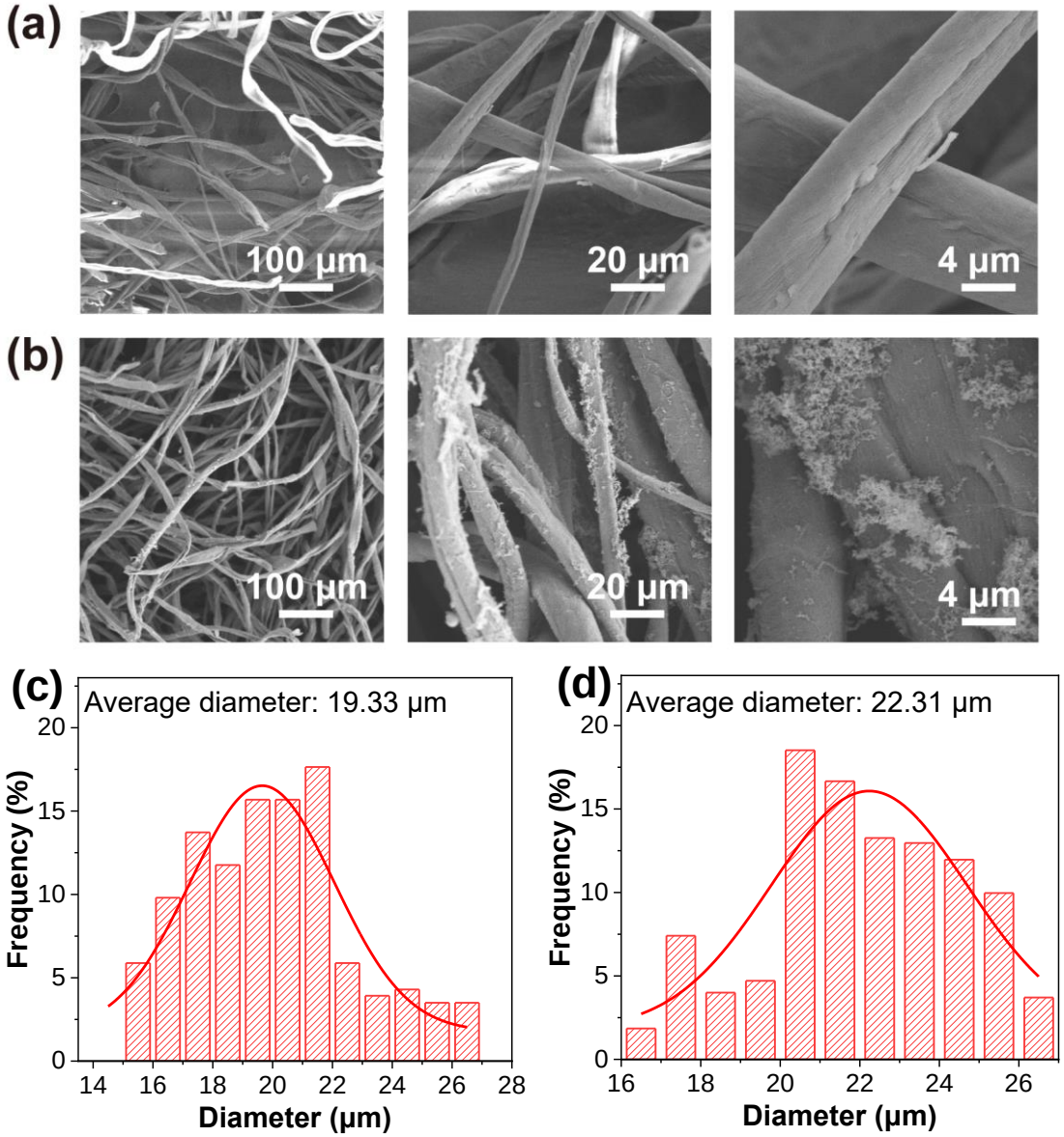

Figure S5. Cross-sectional SEM images of (a) NC films and (b) P-NC films. Corresponding diameter statistical distribution histograms of (c) NC films and (d) P-NC films.

9. Porosity characterization

Porosity (P) refers to the percentage of pore volume to total volume of an aerogel. Based on Archimedes' law, it can be calculated by using Equation S1,

$$P = \frac{V_{pore}}{V_{pore} + V_{displaced}} = \frac{m_2 - m_1}{m_2 - m_1 + \frac{F_b}{g}} \qquad \text{(S1)}$$

where m_1 and m_2 are dry and water-saturated weights of film, respectively. F_b is buoyant force of film, which can be measured by a density meter, and g is the gravitational acceleration (9.8 m s^{-2}).

a) NC film

m_1 = 0.326 g, m_2 = 2.934 g, F_b = 2.626 mN, P = 90.1%

b) P-NC film

m_1 = 0.346 g, m_2 = 3.094 g, F_b = 4.390 mN, P = 86.0%

10. X-ray photoelectron spectroscopy (XPS) measurements

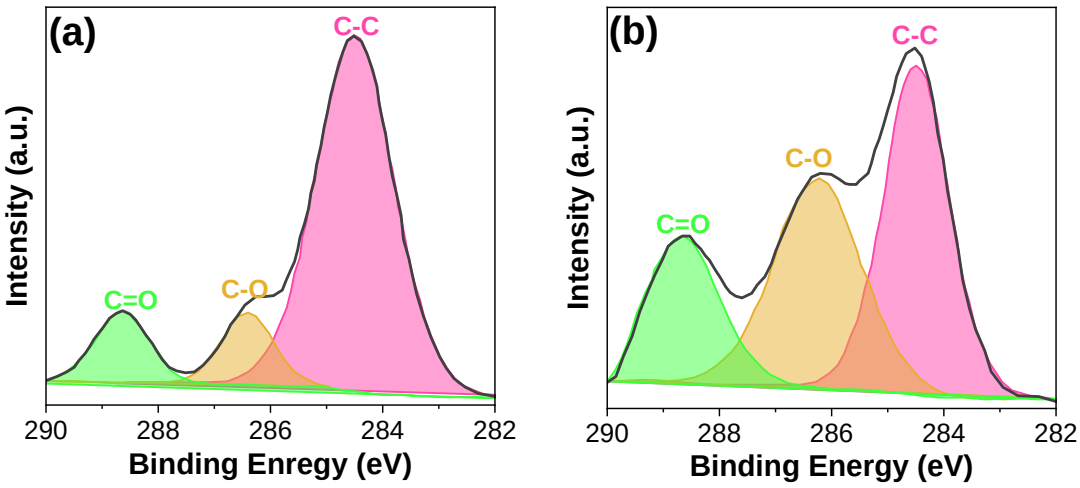

Figure S6. XPS spectra of (a) pristine and (b) O_2 plasma-treated P-NC films.

11. Water contact angle (CA) measurements

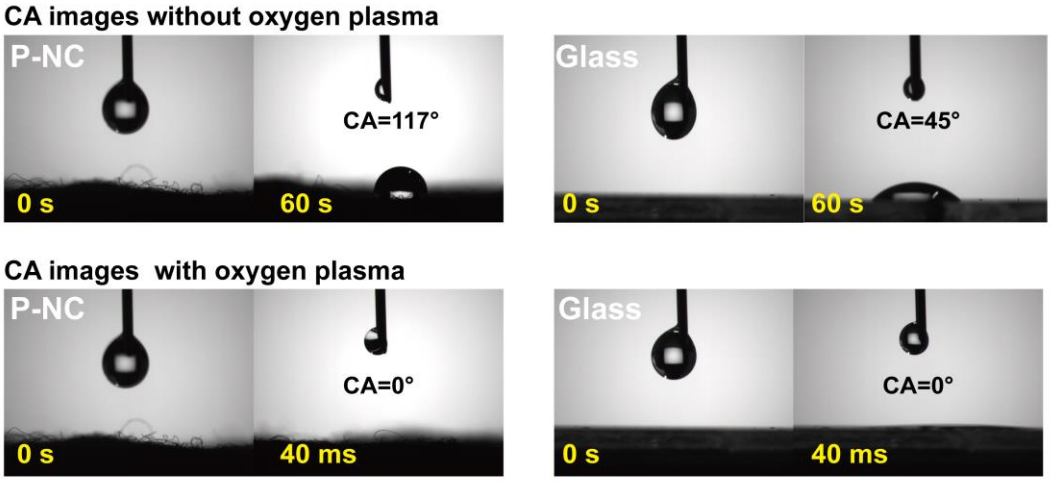

Figure S7. CA measurements of P-NC films and glass slices (used for encapsulation of PSCs).

12. Thermal conductivity measurements

Thermal conductivities of P-NC films were measured via an IR imaging method.[4] The samples with thickness of ~3.1 mm was sandwiched between two 1.1 mm glasses. The sandwich structure was placed between copper plate heated via a solar simulator and a heat sink. The heat transfer rate (q) permeating the sample was calculated by using the Fourier Equation S2:

$$q = -k_1 \frac{T_2 - T_1}{d_1} = -k \frac{T_3 - T_2}{d_2} \qquad \text{(S2)}$$

where k is the thermal conductivity of the sample, k_1 is the thermal conductivity of glass (1.05 W m^{-1} K^{-1}),[5] T_1, T_2, T_3 are the average temperature at the interface of copper plate-top glass, top glass-sample, sample-bottom glass, respectively.

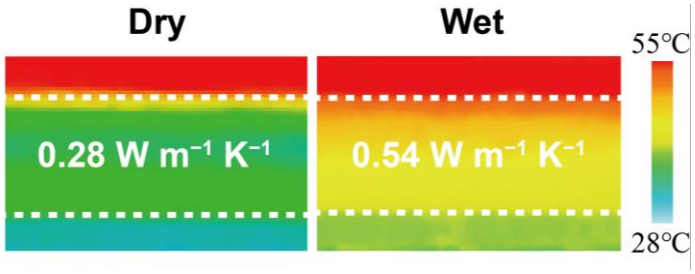

Figure S8. Thermal conductivity measurements of P-NC films in dry and wet states.

13. Tensile stress−strain measurements

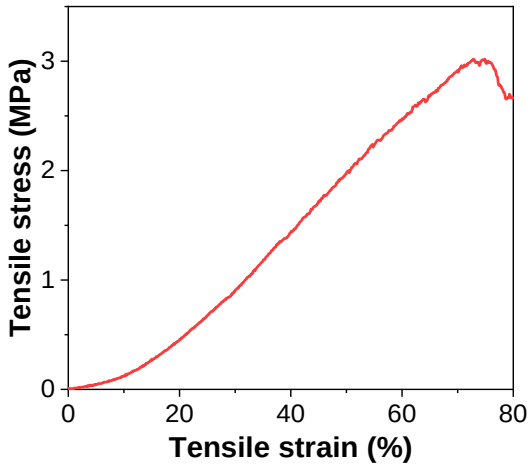

Figure S9. Tensile stress−strain curves of the PN-C film.

14. Transmittance spectra of materials

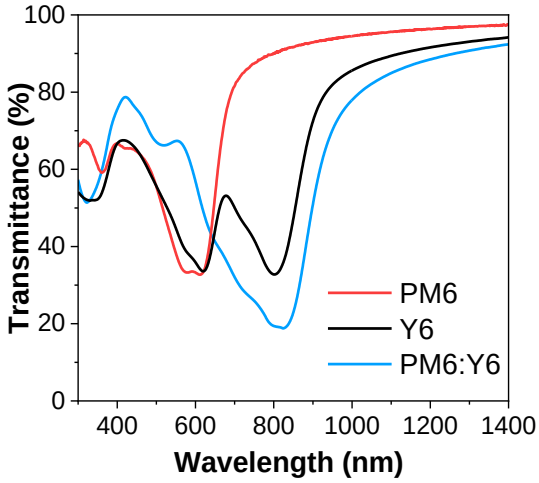

Figure S10. Transmittance spectrum of PM6, Y6 and the blend film.

15. Fabrication of opaque PSCs and ST-PSCs

All PSCs were fabricated and tested in a glove box with temperature: ~22 °C, oxygen: ~0.1 ppm and water: ~0.1 ppm. The PSC with a conventional structure of ITO/PEDOT:PSS(CLEVIOS™ P VP AI 4083)/active layer/PDINO/Ag, where PM6 was chosen as the donor material and Y6 was used as an acceptor. The ITO-coated glass substrates were cleaned by detergent, deionized water and isopropyl alcohol under ultrasonication for 10 min each and then dried with nitrogen blow. After 3 min UV ozone treatment, PEDOT:PSS was spin-coated on ITO at 4000 rpm for 30 s and thermal-annealed at 150 °C for 15 min. The PM6:Y6 was optimized at a 1:1.2 wt% ratio and was spin-coated using a CF solution containing 0.5 vol% of 1-chloronapthalene (CN). The total concentration of solution was fixed as 16 mg/mL. The blend film was spin-coated at 4000 rpm for 30 s and thermal-annealed at 110 °C for 10 min. Then, a methanol solution of PDINO (1 mg/ml) was spin-coated on the active layer at 3000 rpm for 25 s. Finally, Ag (80 nm) was deposited on PDINO via a mask under 3×10^{-4} Pa vacuum. ST-PSCs were fabricated by following a similar procedure with opaque PSCs, where a 15 nm of Ag layer was deposited as top electrode in each device. All PSCs were encapsulated by using ultraviolet-curing epoxy resins and glass slices.

16. Device structures and SEM images

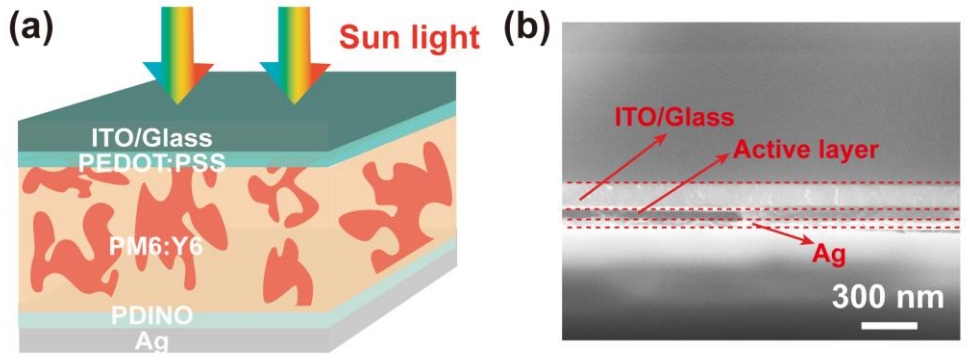

Figure S11. (a) Device structure and (b) a cross-sectional SEM image of an opaque PSC.

17. CIE chromaticity diagram

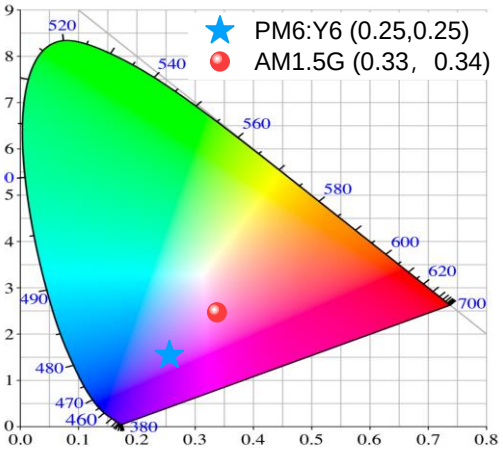

Figure S12. CIE chromaticity diagram exhibiting color coordinates of PM6:Y6 based ST-PSC.

18. Water evaporation rates and photothermal conversion efficiencies

Water evaporation rates (v) was calculated by using Equation S3,[6]

$$v = \frac{\Delta m}{A \cdot t} \qquad \text{(S3)}$$

Where Δm is the mass changes over time (kg); A is the water surface area (m^2) and t is the time of illumination (h).

The photothermal conversion efficiency (η) was calculated by using Equation S4,[7]

$$\eta = \Delta m \, H_{lv} / P_{in} \qquad \text{(S4)}$$

Where Δm is the mass flux of vapor (kg m^{-2} h^{-1}) ($\Delta m = m_{Light} - m_{Dark}$), H_{lv} is the liquid-vapor phase change enthalpy ($H_{lv} = L_v + Q$). L_v is the latent heat of vaporization of water, $L_v = 1.91846 \times 10^6 [T/(T-33.91)]^2$, where T is the temperature of vaporization. Q is the sensible heat of water of unit mass ($Q = c\,(T_2 - T_1)$), in which c is the specific heat of water and can be assumed as a constant (4.2 J g^{-1} K^{-1}), T_2 is the temperature of vaporization and T_1 is the initial temperature of the water. P_{in} is the intensity of the incident sunlight (1000 W m^{-2}).

19. Water evaporation characterization in the dark

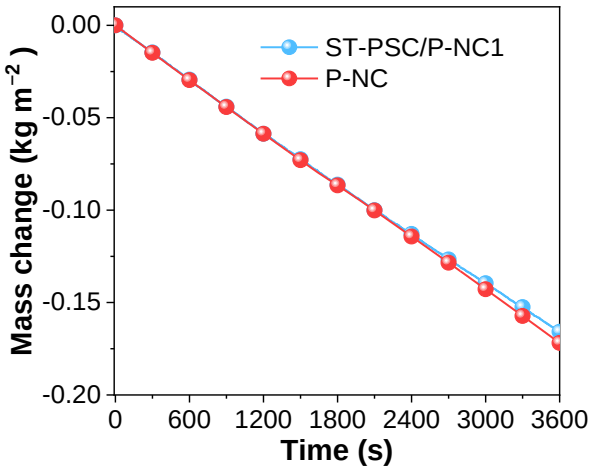

Figure S13. Mass changes of water over time in the dark.

20. Summary of synergistic water-electricity production

Table S1. Summary of water evaporation rates and electricity generation

Water-electricity generation	Interfacial water evaporation [a]		Electricity generation [a]		
	Evaporation rates (kg m^{-2} h^{-1})	Photothermal efficiencies (%)	Energy harvesting materials	Power density (W m^{-2})	Ref.
Photovoltaic	>1.64 (1.64)[b]	126	polysilicon	115.5	8
	0.80	74.6	polysilicon	204	9
	2.61 (1.08)	97.4	silicon	200	10
	0.30	20	ST-PSC	64	11
	0.63	42.9	ST-PSC	130	12
	1.15 (1.10)	75.0	Ag/AgCl	1	13
	1.40	88.9	Ag/AgCl	1.1	14
Salinity gradient power	1.60	91	CB-SDBS	6.75×10^{-3}	15
	1.3	83	carbon cloth/graphene	/	16
	1.15	/	CNT/PDMS	4.83×10^{-4}	17
	1.87	90.8	PVDF	1.54×10^{-2}	18
	2.07	80.2	Cu-CAT-1	1.82×10^{-2}	19
Thermoelectric	1.35	87.4	Bi_2Te_3	0.4	20
	1.26	81	Bi_2Te_3	0.4	21
	31.6 [c]	72.7	Bi_2Te_3	292.9 [c]	22
	0.92	58.6	Bi_2Te_3	0.22	23
	1.72	90	Bi_2Te_3	0.5	24
Pyro-piezoelectric	1.39 (1.15)	90	PVDF	2.41×10^{-4}	25
Thermogalvanic	1.33 (1.12)	91.4	Cu/Cu^{2+}	1.57×10^{-3}	26
	1.1	60	I_3^-/I^- pairs	$\sim0.5\times10^{-3}$	27

[a] Water evaporation and electricity generation were measured under 1 sun unless otherwise specified. [b] Water collection rates are given in the parentheses. [c] measured under 30 sun.

21. Long-term water evaporation measurements

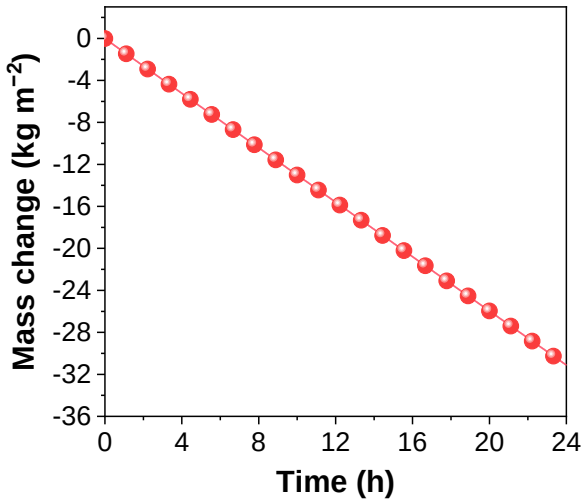

Figure S14. Mass changes of water over 24 h under 1 sun.

22. Stability characterization of ST-PSC

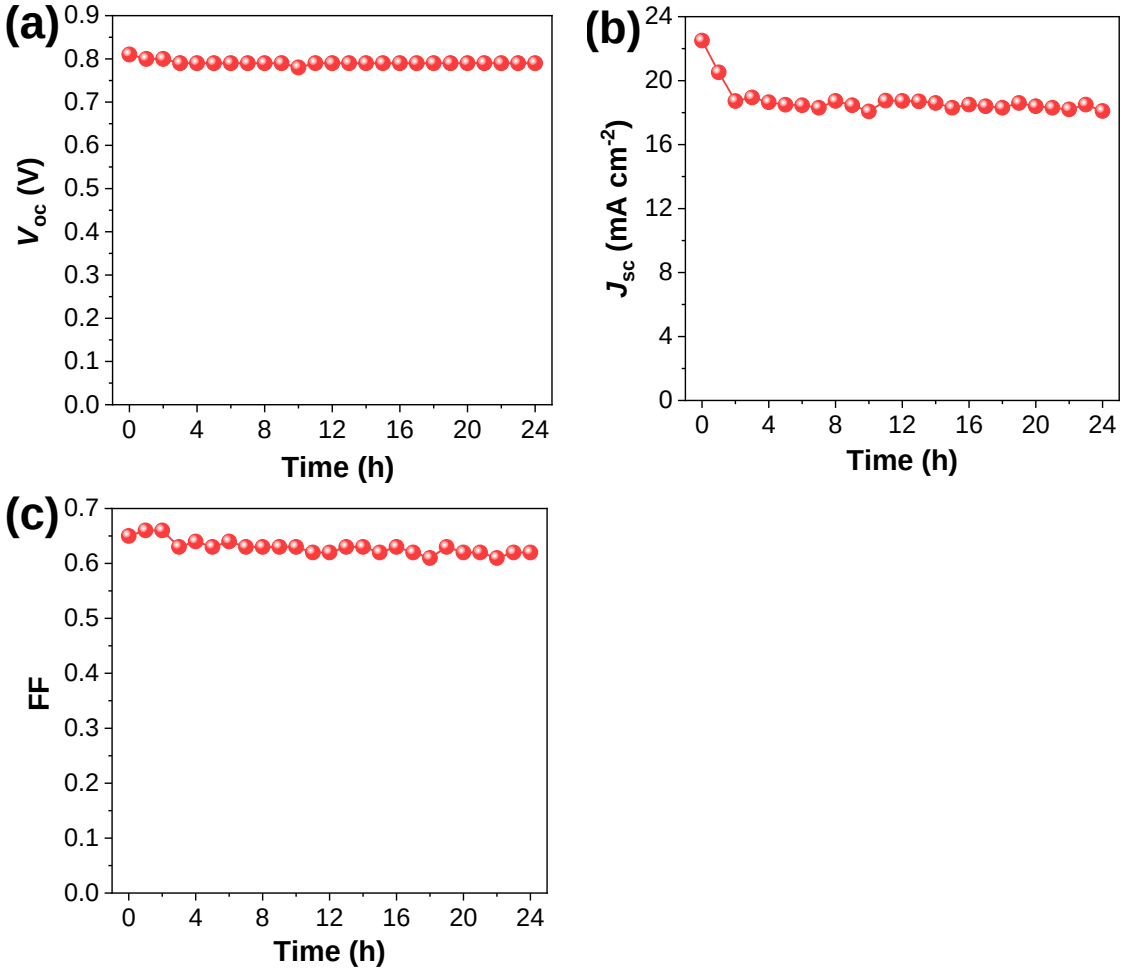

Figure S15. Decay on photovoltaic parameters of ST-PSCs over 24 h under 1 sun.

23. Biofouling characterization

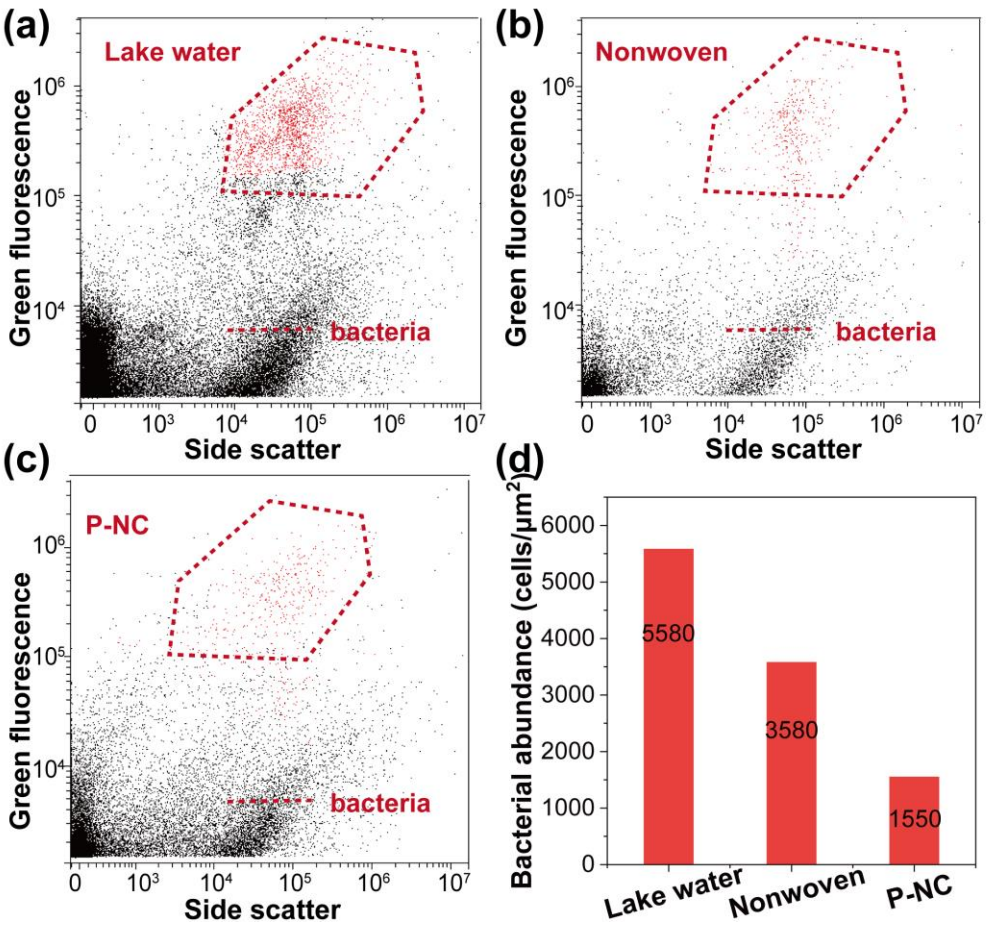

Figure S16. Biofouling characterization in (a) lake water; (b) pristine nonwoven; (c) P-NC film and (d) summary of bacterial concentration.

24. Salt rejection characterization

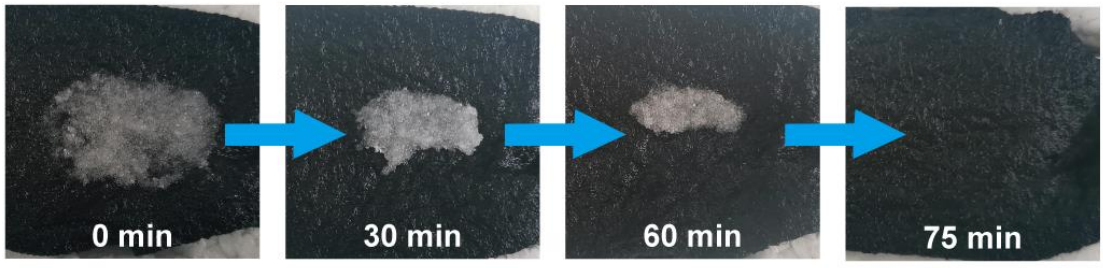

Figure S17. Dissolution of salt crystals on top of P-NC.

25. ICP-MS measurements

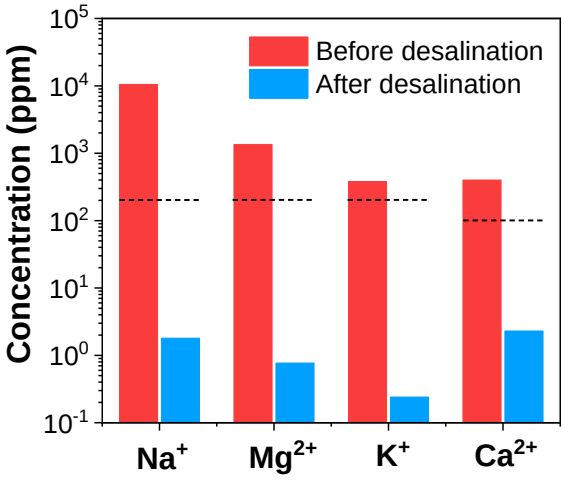

Figure S18. Ion concentration before and after desalination (The black lines show WHO quality standards required for drinking water).

26. Solar energy transfer and energy loss characterization

i) Optical loss (Reflection):

The reflection loss is calculated by using Equation S5,

$$R = \frac{\int R(\lambda)S(\lambda)d\lambda}{\int S(\lambda)d\lambda} \qquad \text{(S5)}$$

where λ is the wavelength range of 300−2500 nm, R is the reflectance spectrum, and S is the incident flux of the AM 1.5G solar spectrum.

ii) Heat loss:

a) Radiative loss:

The radiation flux is calculated by using Stefan-Boltzmann law (S6),[28,25]

$$P_{rad} = \varepsilon\delta\left(T_1^4 - T_2^4\right) \qquad \text{(S6)}$$

where ε is the emissivity (ε=0.93); δ represents the Stefan-Boltzmann constant (δ=5.670373×10^{-8} $W\,m^{-2}\,K^{-4}$); T_1 is the surface temperature of PSCs. T_2 is the temperature of

the adjacent environment.

b) Convective loss:

The convection loss is calculated by using Newton's law of cooling (S7),[28,29]

$$P_{conv} = h\,(T_1 - T_2) \qquad \text{(S7)}$$

where h is convection heat transfer coefficient (assumed to be 5 $W\,m^{-2}\,K^{-1}$); T_1 is the surface temperature of PSCs. T_2 is the temperature of the adjacent environment.

c) Conduction (Heat transfer):

The conduction heat transferred from PSCs to P-NC is calculated by using Equation S8−S10,[8]

$$Q_A = \alpha\, Q_S \qquad \text{(S8)}$$

$$Q_e = \eta\, Q_A \qquad \text{(S9)}$$

$$Q_h = Q_A - Q_e \qquad \text{(S10)}$$

where Q_s is the intensity of the incident sunlight (1000 W m^{-2}); Q_A is the solar energy that was captured by PSCs depending on its solar absorptance α ($\alpha = 1-T-R$); Q_e is the solar energy that was converted to electricity depending of the efficiencies of PSCs (η); Q_h represents the rest of the absorbed solar energy that was converted to heat.

27. Reflectance spectra of devices

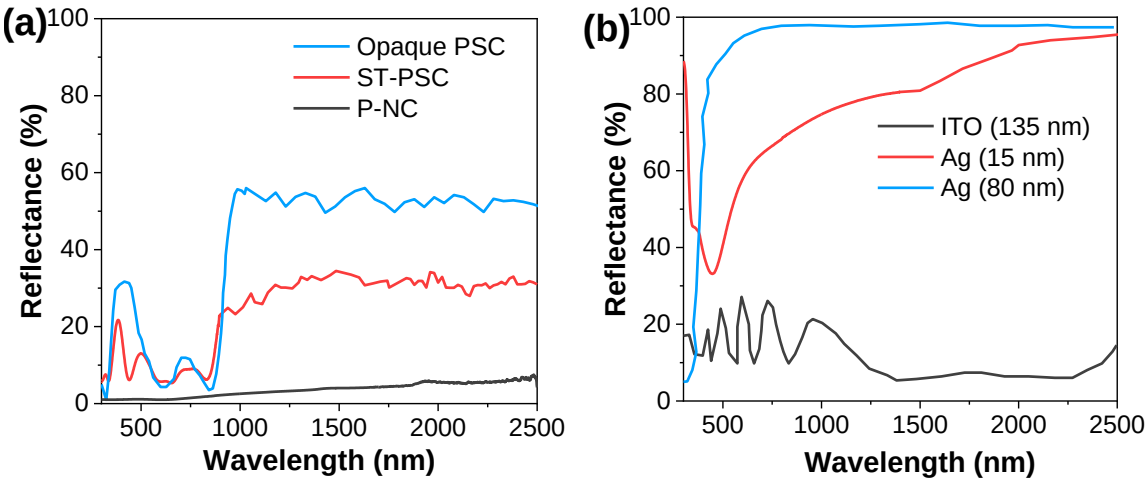

Figure S19. Reflection spectrum of (a) devices and (b) ITO and Ag with different thickness.

28. Transmittance spectra of ITO and Ag electrodes

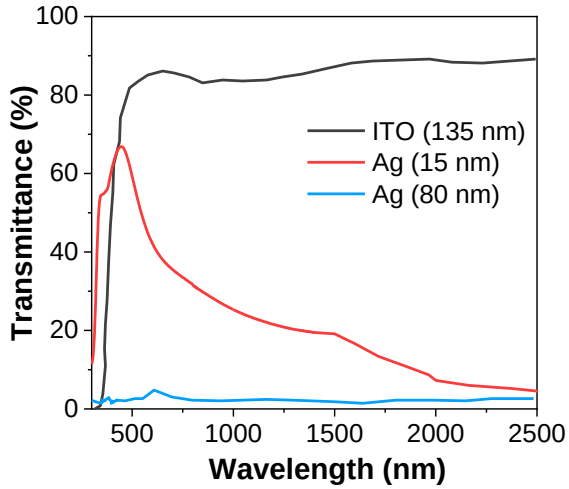

Figure S20. Transmittance spectrum of ITO and Ag with different thickness.

29. Water evaporation measurements of ST-PSC/P-NC2.

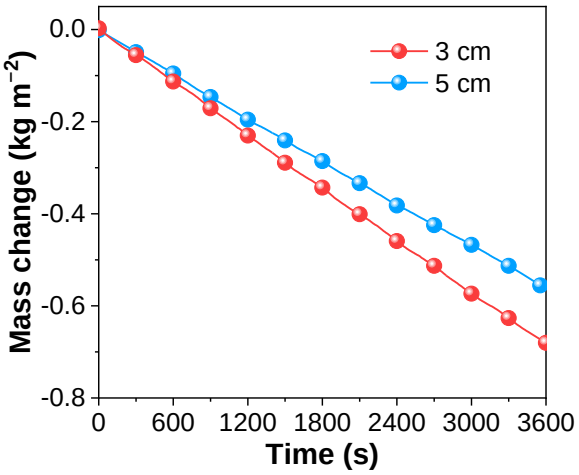

Figure S21. Water evaporation rate of hybrid devices containing different distances between ST-PSC and P-NC (measured under 1 sun).

30. Solar energy budgets in ST-PSC/P-NC2

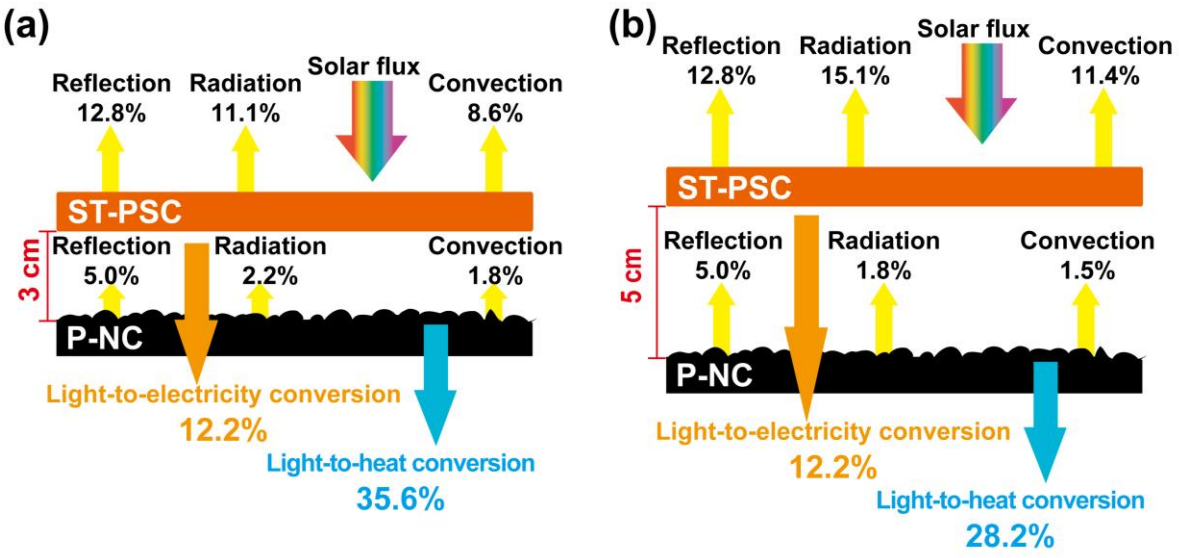

Figure S22. Detailed analysis of the energy flows in the hybrid devices containing different distances between ST-PSC and P-NC.

31. Near-infrared (IR) images

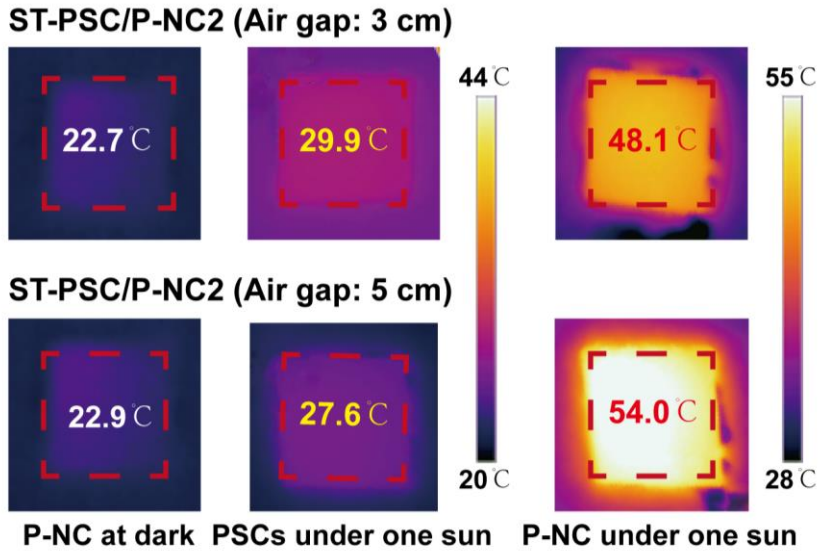

Figure S23. IR images of hybrid devices containing different distances between ST-PSC and P-NC (measured under 1 sun).

32. Reference

1. D. P. Qian, L. Ye, M. J. Zhang, Y. R. Liang, L. J. Li, Y. Huang, X. Guo, S. Q. Zhang, Z. A. Tan and J. H. Hou, *Macromolecules*, 2012, **45**, 9611-9617.
2. M. J. Zhang, X. Guo, W. Ma, H. Ade and J. H. Hou, *Adv. Mater.*, 2015, **27**, 4655-4660.
3. P. Xiao, J. Gu, C. Zhang, F. Ni, Y. Liang, J. He, L. Zhang, J. Ouyang, S.-W. Kuo and T. Chen, *Nano Energy*, 2019, **65**, 104002.
4. H. R. Li, Y. R. He, Y. W. Hu and X. Z. Wang, *ACS Appl. Mater. Interfaces*, 2018, **10**, 9362-9368.
5. J. L. Wan, A. W. Fan, H. Yao and W. Liu, *Energ. Convers. Manage.*, 2015, **96**, 605-612.
6. Z. Y. Deng, J. H. Zhou, L. Miao, C. Y. Liu, Y. Peng, L. X. Sun and S. Tanemura, *J. Mater. Chem. A*, 2017, **5**, 7691-7709.
7. X. Q. Li, G. Ni, T. Cooper, N. Xu, J. L. Li, L. Zhou, X. Z. Hu, B. Zhu, P. C. Yao and J. Zhu, *Joule*, 2019, **3**, 1798-1803.
8. W. B. Wang, Y. Shi, C. L. Zhang, S. Hong, L. Shi, J. Chang, R. Y. Li, Y. Jin, C. Ong, S. F. Zhuo and P. Wang, *Nat. Commun.*, 2019, **10**, 3012.
9. N. Xu, P. Zhu, Y. Sheng, L. Zhou, X. Li, H. Tan, S. Zhu and J. Zhu, *Joule*, 2020, **4**, 347-358.
10. L. F. Cui, P. P. Zhang, Y. K. Xiao, Y. Liang, H. X. Liang, Z. H. Cheng and L. T. Qu, *Adv. Mater.*, 2018, **30**, 1706805.
11. N. Zhang, G. Chen, Y. Xu, X. Xu and L. Yu, *ACS Appl. Energy Mater.*, 2019, **2**, 6060-6070.
12. N. Zhang, T. Jiang, C. Guo, L. Qiao, Q. Ji, L. Yin, L. Yu, P. Murto and X. Xu, *Nano Energy*, 2020, **77**, 105111.
13. P. Yang, K. Liu, Q. Chen, J. Li, J. Duan, G. Xue, Z. Xu, W. Xie and J. Zhou, *Energy. Environ. Sci.*, 2017, **10**, 1923-1927.
14. H. Wang, W. Xie, B. Yu, B. Qi, R. Liu, X. Zhuang, S. Liu, P. Liu, J. Duan and J. Zhou, *Adv. Energy Mater.*, 2021, **11**, 2100481.

15. Y. Zhang, H. Zhang, T. Xiong, H. Qu, J. J. Koh, D. K. Nandakumar, J. Wang and S. C. Tan, *Energy. Environ. Sci.*, 2020, **13**, 4891-4902.
16. B. F. Hou, D. N. Kong, J. W. Qian, Y. Yu, Z. Q. Cui, X. H. Liu, J. Y. Wang, T. Mei, J. H. Li and X. B. Wang, *Carbon*, 2018, **140**, 488-493.
17. P. Xiao, J. He, F. Ni, C. Zhang, Y. Liang, W. Zhou, J. Gu, J. Xia, S.-W. Kuo and T. Chen, *Nano Energy*, 2020, **68**, 104385.
18. Z. Li, X. Ma, D. Chen, X. Wan, X. Wang, Z. Fang and X. Peng, *Adv. Sci.*, 2021, **8**, 2004552.
19. X. Ma, Z. Li, Z. Deng, D. Chen, X. Wang, X. Wan, Z. Fang and X. Peng, *J. Mater. Chem. A*, 2021, **9**, 9048-9055.
20. L. L. Zhu, T. P. Ding, M. M. Gao, C. K. N. Peh and G. W. Ho, *Adv. Energy Mater.*, 2019, **9**, 1900250.
21. Y. X. Zhang, S. K. Ravi and S. C. Tan, *Nano Energy*, 2019, **65**, 104006.
22. X. Q. Li, X. Z. Min, J. L. Li, N. Xu, P. C. Zhu, B. Bin Zhu, S. N. Zhu and J. Zhu, *Joule*, 2018, **2**, 2477-2484.
23. X. F. Zhang, W. Q. Gao, X. W. Su, F. L. Wang, B. S. Liu, J. J. Wang, H. Liu and Y. H. Sang, *Nano Energy*, 2018, **48**, 481-488.
24. L. Zong, M. J. Li and C. X. Li, *Nano Energy*, 2018, **50**, 308-315.
25. L. L. Zhu, M. M. Gao, C. K. N. Peh, X. Q. Wang and G. W. Ho, *Adv. Energy Mater.*, 2018, **8**, 323-343.
26. F. L. Meng, M. M. Gao, T. P. Ding, G. Yilmaz, W. L. Ong and G. W. Ho, *Adv. Funct. Mater.*, 2020, **30**, 2002867.
27. Q. C. Shen, Z. Y. Ning, B. W. Fu, S. Ma, Z. Y. Wang, L. Shu, L. F. Zhang, X. Y. Wang, J. L. Xu, P. Tao, C. Y. Song, J. B. Wu, T. Deng and W. Shang, *J. Mater. Chem. A*, 2019, **7**, 6514-6521.
28. F. Ni, P. Xiao, N. X. Qiu, C. Zhang, Y. Liang, J. C. Gu, J. Y. Xia, Z. X. Zeng, L. P. Wang, Q. J. Xue and T. Chen, *Nano Energy*, 2020, **68**, 104311.
29. H. Ghasemi, G. Ni, A. M. Marconnet, J. Loomis, S. Yerci, N. Miljkovic and G. Chen, *Nat. Commun.*, 2014, **5**, 4449.